Nanoscale

PAPER

Reduced graphene oxide growth on 316L stainless steel for medical applications

Cite this: *Nanoscale*, 2014, **6**, 8664

L. Cardenas,*[ab] J. MacLeod,[a] J. Lipton-Duffin,[a] D. G. Seifu,[b] F. Popescu,[c] M. Siaj,[c] D. Mantovani[b] and F. Rosei*[ad]

Received 8th May 2014
Accepted 3rd June 2014

DOI: 10.1039/c4nr02512a

www.rsc.org/nanoscale

We report a new method for the growth of reduced graphene oxide (rGO) on the 316L alloy of stainless steel (SS) and its relevance for biomedical applications. We demonstrate that electrochemical etching increases the concentration of metallic species on the surface and enables the growth of rGO. This result is supported through a combination of Raman spectroscopy, X-ray photoelectron spectroscopy (XPS), atomic force microscopy (AFM), scanning electron microscopy (SEM), density functional theory (DFT) calculations and static water contact angle measurements. Raman spectroscopy identifies the G and D bands for oxidized species of graphene at 1595 cm^{-1} and 1350 cm^{-1}, respectively, and gives an I_D/I_G ratio of 1.2, indicating a moderate degree of oxidation. XPS shows –OH and –COOH groups in the rGO stoichiometry and static contact angle measurements confirm the wettability of rGO. SEM and AFM measurements were performed on different substrates before and after coronene treatment to confirm rGO growth. Cell viability studies reveal that these rGO coatings do not have toxic effects on mammalian cells, making this material suitable for biomedical and biotechnological applications.

Introduction

The fabrication of implantable devices exhibiting superior corrosion and high mechanical resistance properties has been the focus of extensive efforts during the past decades.[1,2] Stainless steel 316L (SS316L) is one of the most commonly used materials for the fabrication of implantable devices. SS316L is used extensively in coronary/cardiovascular stents,[3,4] cranial fixation,[5] orthopedic stents[6,7] and dental implants.[8,9] However, it exhibits limited resistance to corrosion and wear, which can lead to degradation of the material and its subsequent release of potential harmful metallic ions, thereby contributing to clinical complications such as thrombus and apoptosis.[10] Although SS316L is natively covered with a passivating layer of metal oxides, this is not sufficient to protect it against localized forms of corrosion (pitting) associated with chloride ions in aqueous environments.[11] The human body is not a friendly environment for implanted materials, mostly due to the presence of highly oxygenated saline electrolyte, which can cause the corrosion and subsequent degradation of SS316L.[12] In addition, physiological conditions exert pressure/friction against the surface of medical devices, requiring high mechanical resistance to wear.

Coating SS316L with a protective layer can improve its mechanical and anticorrosive properties. Graphene (Gr) and related materials could be excellent candidates as protective coatings, since they exhibit extraordinary mechanical[13] and anticorrosion[14] properties. Stiffness and strength are the key factors in determining the stability and lifetime of medical devices. Gr is one of the strongest known materials, possessing an ultrahigh Young's modulus of ~1 TPa and an intrinsic fracture strength of ~130 GPa.[13] Extensive efforts have been devoted to the study of the effects of growing or attaching Gr layers over corrosion-prone surfaces, such as copper and nickel. These studies have demonstrated that Gr coatings grown by chemical vapour deposition provide significant corrosion protection as compared to the bare metallic substrates.[14,15] More recently, other studies suggest that Gr is an effective oxidation inhibitor on copper,[16,17] and silicon,[17] albeit over short time scales only (*ca.* 1 month). Gr coatings inhibit oxidation because they are impermeable to all standard gases.[18] These mechanical and anticorrosive properties make Gr an excellent candidate for the fabrication of protective layers on SS316L for implantable devices.

In addition to having excellent physical and chemical properties, Gr is also gathering interest in the biomedical field,[19] where it is used as a new component in biosensors,[20,21] tissue engineering[22,23] and drug delivery.[24,25] Most biological tests, including biological response and safety tests, have been

[a]*INRS-Centre Énergie, Matériaux et Télécommunications, Boulevard Lionel-Boulet, Varennes, Québec, J3X 1S2, Canada. E-mail: luis.cardenas@ircelyon.univ-lyon1.fr; rosei@emt.inrs.ca*

[b]*Laboratory for Biomaterials and Bioengineering, CRC-I, Department of Mining, Metallurgical and Materials Engineering & Research Center of CHU de Québec, Laval University, Quebec City, QC, G1V 0A6, Canada*

[c]*Département de Chimie et Biochimie, Université du Québec à Montréal, Montréal, QC H3C 3P8, Canada*

[d]*Center for Self-Assembled Chemical Structures, McGill University, H3A 2K6 Montreal, Quebec, Canada*

conducted on reduced Gr oxide (rGO) and Gr oxide (GO). This is because rGO and GO are more hydrophilic than pristine Gr. This hydrophilicity renders rGO and GO soluble in water and allows them to remain stably dispersed,[26] thus improving their potential to act as surface coatings with improved biocompatibility. Coating SS316L with an oxidized form of Gr could produce a material useful for a broad range of biomedical applications, especially when considering the possibility of controlling its properties such as available reactive oxygen species, surface area, cytotoxicity and corrosion resistance.

Here, we present a new method for synthesizing rGO directly on SS316L.[27] Our approach is scalable and produces rGO coatings that foster good cell viability and stability.

Materials and methods

Electropolishing of SS316L

Single-side mirror polished SS316L foils (Goodfellow Cambridge Limited, thickness 0.9 mm) were used as the anode of an electrochemical cell, while a copper plate was used as cathode. The electrolyte solution was a mixture of 8 parts by volume of orthophosphoric acid (85%, Fisher Scientific), 2 parts distilled deionized water, and 1 part sulphuric acid (98%, ReAgent supplies). The voltage was kept constant at 3.8 V, with a current density of 5×10^{-3} mA mm^{-2}, with a total electropolishing time of 5 min. Following electropolishing, the SS316L foil was cleaned by sonication in ethanol.

Preparation of rGO coating

Coronene (97%, Sigma Aldrich) was dissolved in trichlorobenzene (TCB, 99%, Sigma-Aldrich) at a concentration between 10^{-4} and 10^{-5} M. The coronene solution was drop cast onto electropolished SS316L. Samples were heated between 600 °C and 800 °C for 30 minutes under a flowing atmosphere of 98% nitrogen and 2% hydrogen in a quartz tube.[28] After annealing, the furnace was cooled over 10 min while maintaining the N_2/H_2 flow.

Characterization methods

Raman spectroscopy was performed in the region of 800–3500 cm^{-1} using an inVia Raman microscope (Renishaw with a laser wavelength of 514 nm). Scanning with this instrument was used to evaluate the presence and uniformity of rGO on the SS316L. X-ray photoelectron spectroscopy (XPS) was performed using a Mg K_α source in a commercial instrument (VG ESCALAB 220i XL), and revealed well-resolved peaks corresponding to C 1s, O 1s, Ni 2p, Cr 2p, and Fe 2p core levels. Each high-resolution spectrum was decomposed into a combination of Voigt functions, each with an overall full-width at half maximum (FWHM) of approximately 1.4 eV. ScanAsyst mode atomic force microscopy (AFM) using an Agilent 5500 microscope was employed to study *in situ* the changes of the sample surfaces before and after rGO growth. Topography images are recorded in ScanAsyst mapping mode using Si cantilevers with a spring constant of 0.2 N m^{-1} and typical radius of about 20–25 nm. AFM topography images were analyzed using WSxM software.[29]

Static contact angle measurements were carried out using a homemade injection system; 10 μL of deionized water was deposited on rGO through a 160 μm diameter capillary. The images were analyzed and treated using the ImageJ software[30] with the LBADSA plugin.[31]

Ab initio calculations

Density functional theory (DFT) calculations were carried out to identify the vibrational frequencies and Raman intensities for the coronene monomer, dimer and trimer configurations. Calculations were performed using Gaussian 09 (ref. 32) by DFT at the B3LYP level[33] using the 6-31G basis set.

Cell toxicity experiments

The different samples were placed in six-well culture plates (SARSTEDT Inc. Newton, NC, USA). After fixing the samples in the well they were sterilized using 70% ethanol, washed with 1× phosphate buffered saline (1×PBS) twice, UV was applied for 2 h on both sides and finally they were again washed with 1×PBS twice. Subsequently the samples were incubated at 4 °C overnight with 1 ml culture medium on a shaker. At the same time 2.5 × 104 human umbilical vein endothelial cells (HUVECs) were seeded on 96-wall tissue culture plate (SARSTEDT Inc. Newton, NC, USA) and the cells were allowed to grow for 24 h. Afterwards the medium was replaced by the medium incubated 24 h with the samples and cells were further allowed to grow for 24 h. Finally, the cellular viability was quantified using resazurin as a redox indicator. Resazurin (7-hydroxy-3*H*-phenoxazin-3-one 10-oxide) is a fluorescent common dye marker used as an indicator for cell viability in HUVEC cultures. Resazurin fluoresces and changes color in response to the chemical reduction of the culture medium, resulting from cell growth. In this process the resazurin[34,35] is irreversibly reduced to resorufin.[35]

Results and discussion

XPS reveals that electrochemical polishing of bare SS316L enriches the surface content of metallic nickel, iron and chromium. Spectra are shown in Fig. 1 for the Ni 2p3/2, Fe 2p3/2 and Cr 2p3/2 core levels for unpolished SS316L polished SS316L samples. The surface of the untreated sample has no detectable nickel, nor any metallic states of iron or chromium at the surface. However, the spectra for treated SS316L reveal a significant nickel concentration (9.4%) at the surface, with two well-resolved contributions and a shoulder. These features may

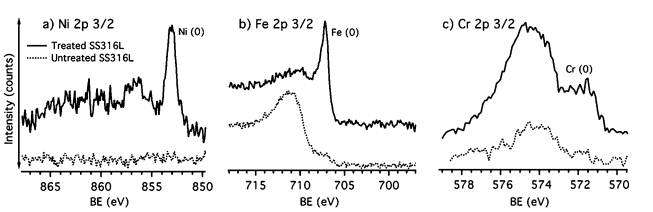

Fig. 1 XPS spectra of Ni 2p3/2, Fe 2p3/2, Cr 2p3/2 for untreated SS316L (below) and treated SS316L (above).

be assigned as metallic nickel (853.2 eV), and nickel(II) oxide (856.6 eV). Likewise, iron and chromium increase in concentration at the surface to 42.4% and 48.0% respectively, including metallic states corresponding to Fe(0) at 707 eV and Cr(0) at 573 eV.

Coronene was applied dropwise from solution to the SS samples, which were subsequently annealed at 800 °C for 30 minutes (see Materials and methods). Coronene was chosen as the precursor based on its relatively high thermo-resistivity: dimerization happens in powder samples between 550 °C and 600 °C.[36] From a structural point of view, coronene is essentially a small flake of graphene, comprising sp^2 carbon formed by six cyclobenzenes (Scheme 1).

Raman spectroscopy has been widely used on carbonaceous systems such as carbon nanotubes,[37] fullerenes,[38] and graphene.[39,40] This powerful technique makes it possible to obtain spectroscopic signatures of hybridized carbon sp^2 bonds present in honeycomb networks. Raman spectra exhibit characteristic bands for these materials; among them are the G line at *ca.* 1585 cm^{-1} and the D band around 1350 cm^{-1}.[39–41] The G band describes a stretching mode attributable to sp^2-hybridized carbon atoms in the honeycomb network.[42] The D band characterizes disordered and amorphous carbon bonds and originates from the breathing mode of *k*-point phonons of A_1 symmetry.[41] At high wavenumbers a series of overtones from both D and G are visible between *ca.* 2700 and 3300 cm^{-1}.[42]

The Raman spectrum of pristine coronene supported on glass (Fig. 2a, blue curve) shows a strong D band at 1359 cm^{-1}, with a small G line at 1600 cm^{-1}. The intensity amplitude ratio I_D/I_G is 7.88, consistent with the relatively small spatial extent of the sp^2 network in coronene. The Raman spectrum for the annealed coronene film on untreated SS316L (Fig. 2a, black curve) has a broader and more intense D band at 1359 cm^{-1}. The G band at 1597 cm^{-1} is virtually non-existent. This suggests that graphene does not grow on the untreated SS316L surface. In the case of the annealed coronene film on treated SS316L (Fig. 2a, red curve) the Raman spectrum exhibits broader and more intense peaks. The G band is shifted to 1597 cm^{-1} whereas the D band appears at 1359 cm^{-1}, in agreement with earlier reports of rGO.[43] The average size of sp^2-bonded graphitic domains is inversely proportional to the I_D/I_G ratio;[44] the ratio I_D/I_G from our samples is approximately 1.2, which is also consistent with ratios reported for other rGO materials.[44] This indicates that the sp^2 network extends much further than it does in the coronene molecule, a clear signature of oligomerization and expansion of the graphene lattice. These results are consistent with the formation of rGO on the treated SS316L surface.

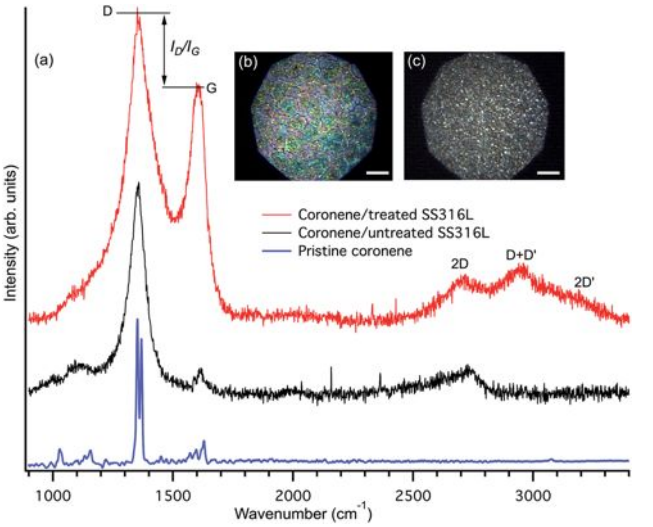

Fig. 2 (a) Raman spectra corresponding to rGO (red curve), coronene on untreated SS316L (black curve) and coronene on glass (blue curve) on the same area where optical images were taken for: (b) rGO/SS316L and (c) coronene/untreated SS316L. Scale bars in the inset images represent 20 μm.

Fig. 2b and c display optical microscopy images of the rGO (coronene/treated SS316L) and the coronene/untreated SS316L samples in the region where the Raman spectra were acquired. Two important features are discernible in the image of the treated sample (Fig. 2b): (i) a colour variation due to the intrinsic reflectance of graphene oxide;[45] and (ii) graphene-like 120° grain boundaries, consistent with previous observations.[46] These features are absent in the image of coronene/untreated SS316L (Fig. 2c).

AFM was used to inspect the surface morphology of untreated SS316L, treated SS316L and rGO/SS316L. Untreated SS316L (Fig. 3a) presents patterns of well-defined grain boundaries characteristic of stainless steel.[47] After treatment (Fig. 3b) the surface becomes considerably smoother. Following the rGO coating, the steel surface becomes populated with multi-layered arrangements of flakes as seen in the AFM image displayed in Fig. 3c. The heights of layered rGO platelets follow a roughly normal distribution with a mean height of 23 ± 2 nm and a standard deviation of 9 ± 2 nm. A clearer illustration of the rGO/SS316L surface is given by the SEM image in Fig. 3d. Flakes completely cover the surface and follow its contour.

DFT at the B3LYP level[33] was used to investigate the theoretical Raman spectra of successive oligomerizations of coronene, in monomer (Fig. 4a, red curve), trimer (Fig. 4a, black curve) and tetramer (Fig. 4a, blue curve) configurations.† The calculated Raman spectrum (Fig. 4a) for a single coronene molecule has D and G bands at *ca.* 1407 cm^{-1} and *ca.* 1656 cm^{-1}

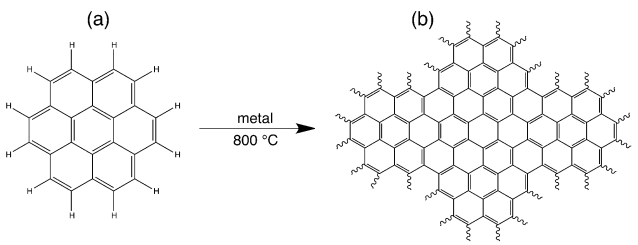

Scheme 1 (a) Molecular model of coronene. (b) Subsequent polymerization of coronene by dehydrogenation and rebonding.

† Note that dimer, trimer and tetramer configurations of coronene are a chemical structure formed from two, three and four identical sub-units of coronene.

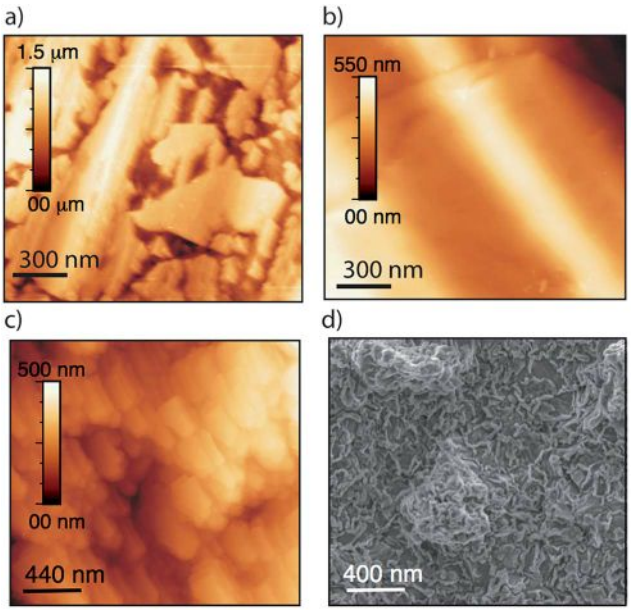

Fig. 3 AFM images on untreated SS316L (a), treated SS316L (b) and rGO/SS316L (c). SEM image on rGO/SS316L (d).

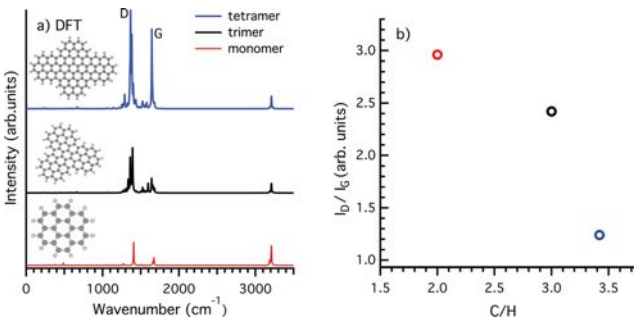

Fig. 4 (a) Calculated Raman spectra for each DFT optimized structures (single-coronene, trimer-coronene and tetramer-coronene). (b) Carbon–Hydrogen (C/H) *vs.* I_D/I_G ratios.

respectively, yielding an I_D/I_G ratio of ~3. Fig. 4b shows the decreasing evolution of the I_D/I_G ratio for successively larger oligomers, consistent with the spatial expansion of the network of sp^2-graphitic bonds.

Fig. 5 shows XPS spectra of the C 1s and O 1s core levels were obtained from the rGO/SS316L, treated SS316L and untreated SS316L samples. The C 1s peak (bottom, Fig. 5a) on untreated/SS316L is broad, with a shoulder at high binding energy. The contribution located at 284.9 eV is attributable to C(sp^3) bonds. The shoulder can be fit with by three contributions, one corresponding to COH groups (pink curve, 286.6 eV), one attributable to CO (light blue curve, 288.1) and the last to –COOH groups (violet curve, 289.0 eV) with a concentration of 2.9%. After treatment, the concentration of COH groups increases significantly and –COOH decreases to a relative concentration of 0.5% (middle, Fig. 5a). Growing rGO on the treated surface reveals a new contribution at 284.3 eV corresponding to C(sp^2) bonds accompanied by the increase of the –COOH contribution

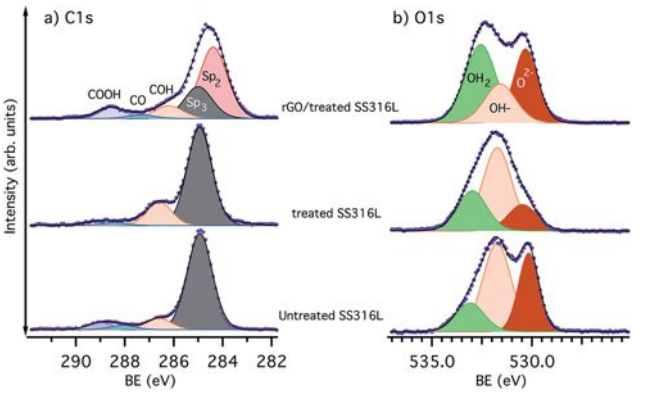

Fig. 5 XPS spectra of (a) C 1s, and (b) O 1s on untreated SS316L, treated SS316L and rGO/SS.

(relative concentration, 4.1%). Fig. 5b shows core level spectra of O 1s for rGO/SS316L, treated and untreated SS316L, which can be fit by three peaks attributable to O^{2-}, hydroxyl groups (OH^-) and hydrate or water (OH_2). The O^{2-} contribution is associated with metallic oxide states on the surface (relative concentration, 33.1%). The O 1s core levels reveal the crucial importance of electrochemical etching through to a pronounced decrease of this contribution (concentration, 18.0%). The top spectrum, of SS with rGO, exhibits a recovered intensity of this O^{2-} contribution with a concentration of 22.5%.

The presence of hydroxyl groups on the rGO is confirmed by both the C 1s and O 1s spectra. These XPS data are consistent with the Lerf and Klinowski model for GO, in which carboxylic acid groups are primarily located on the periphery of the basal plane of platelets of GO, whereas hydroxyl groups are incorporated in the graphene structure.[48] An analysis of the XPS signals shows that these functional groups (–OH– or –COOH) cover about 18% of the surface as compared to 10% for rGO.[59]

Carbon–metal bonds were not detected in the C 1s core level spectrum. In addition, Ni 2p and Fe 2p core level did not appear in the XPS spectra (Fig. 6a and b) after rGO growth. This indicates that these metallic elements, which are of course present in the SS, are buried by the rGO layer and are immiscible. This is an important aspect in relation to biological applications. However, a small amount of oxidized Cr 2p was observed on the rGO/treated SS316L sample (Fig. 6c). This signal (Cr 2p) is consistent with the higher initial concentration of chromium (48%) in treated SS316L, which is visible even after graphene

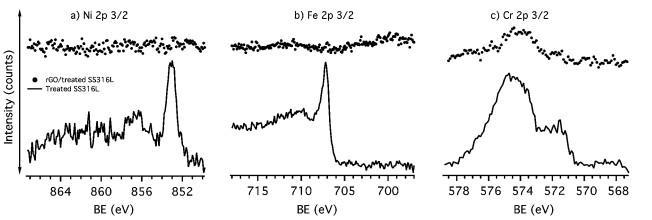

Fig. 6 XPS spectra of Ni 2p3/2, Fe 2p3/2, Cr 2p3/2 for treated SS316L (below) and rGO/treated SS316L (above).

growth on the treated SS316L sample. It has recently been suggested that the presence of metallic chromium on the surface may be detrimental to graphene growth under certain conditions.[50] Our results here show that the presence of chromium oxide does not preclude the growth of the graphene oxide.

The wettability of the rGO layers, along with untreated and treated SS316L samples, was tested by measuring static water contact angles (Fig. 7). The mean static contact angle between rGO/treated SS316L and water was found to be 62 ± 2° (Fig. 7c). Untreated and treated SS316L were used as references, with mean contact angles of 92 ± 2°(Fig. 7a) and 52 ± 2°(Fig. 7b), respectively. The difference between the static water contact angles on untreated and treated SS316L is due to the addition of water molecules to SS316L. This effect, known as hydrolysis, is induced by electrochemical etching.[11] These measurements confirm that the rGO layer improves the SS316L wettability due to its hydroxyl and carboxylic groups, as confirmed by our previous XPS analysis on rGO/SS.

Cell viability of rGO

Cytotoxicity tests were carried out on rGO, treated SS and untreated SS. Human Umbilical Vein Endothelial Cells (HUVECs) growth was used to quantify the cytotoxicity of each sample. HUVECs are sensitive compared to fibroblast and smooth muscle cells, and are the cells that line the inner surface of blood vessels;[51] therefore, they are an extremely pertinent model for testing the cytotoxicity of the rGO/SS316L for vascular and cardiac stent applications.

The Alamar blue assay for HUVECs quantification is a common method for screening the adverse effect of nanomaterials in cell culture.[52] The Alamar blue assay test was performed after 48 h of incubation. The medium was removed from the culture dishes and the adhered cells were washed twice with 1× phosphate buffered saline (1×PBS) and new cell culture media was added to the culture dishes. Afterwards Alamar blue was added directly into the culture medium at a final concentration of 10%. The fluorescence was measured at 540 nm excitation wavelength and 590 nm emission wavelength using a microplate spectrometer (FL600 Microplate Fluorescence Reader, BIO-TEK, Winooski VT, USA). Alamar blue solution was also added to a medium without cells, as a negative control. An Alamar blue containing culture dish with a confluent layer of HUVECs served as a positive control in addition to that pure resorufin absorbance was measured. The measured fluorescence signals are proportional to the number and metabolic activity of the cells. Statistical analysis was performed using the Student's *t*-test ($p < 0.05$) (see Fig. 8).

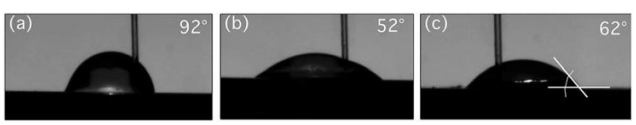

Fig. 7 Water droplet on untreated SS316L (a), treated SS316L (b), and rGO/treated SS316L (c), showing a schematic angle measurement (white lines).

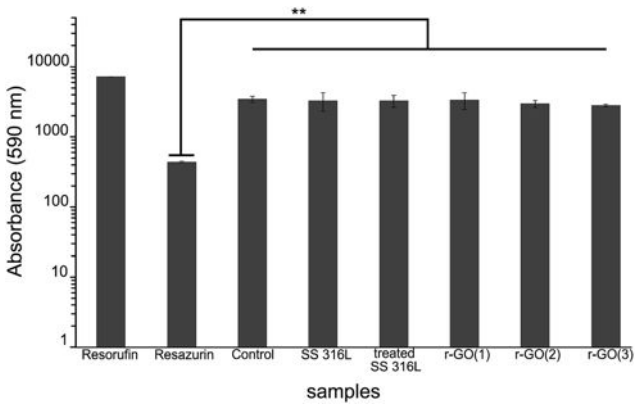

Fig. 8 HUVEC cell viability after exposure to untreated SS316L, treated SS316L and rGO (triple sampling for repeated surveys) based on the Alamar blue assay. Fluorescence signals are proportional to the number and metabolic activity of the cells. Statistical analysis was performed using a Student's *t*-test ($p < 0.05$).

The phase-contrast microscopy images (2D cultures) presented in Fig. 9 demonstrate that the morphology and spreading of cells were not affected compared to the control for all the three samples (rGO, untreated SS and treated SS). The Alamar blue absorbance data presented in Fig. 8 confirmed that none of the samples were toxic to HUVECs. There is no significant difference in the absorbance of resorufin between the control and the three different samples. Our data demonstrate

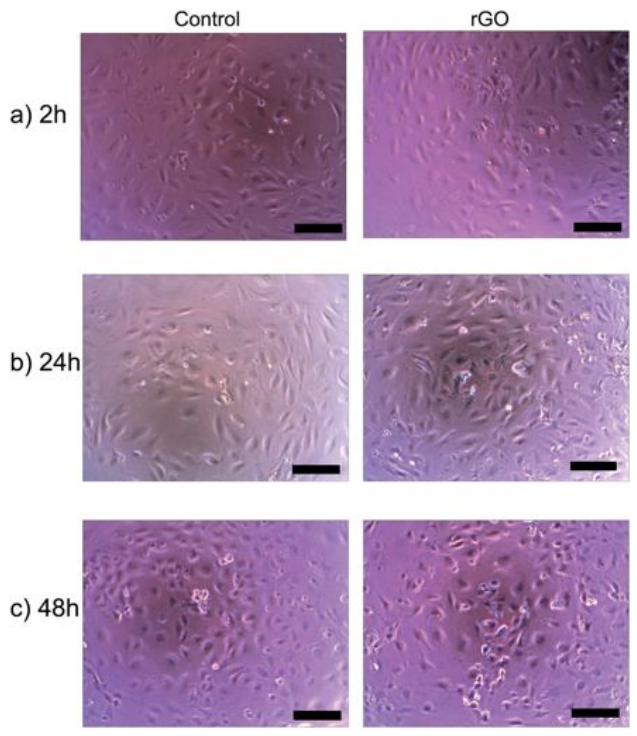

Fig. 9 Phase-contrast microscopy images of cells grown on the control (left) and rGO (right) samples, respectively incubated for: (a) 2 h, (b) 24 h and (c) 48 h. Scale bars in the inset images represent 100 μm.

excellent cell viability when tested with non-contact toxicity for all samples, and indicate that none of the treated samples leached any toxic species into the culture medium when following standard sterilization procedures.

Conclusions

We developed a method for producing a rGO coating on SS316L. The rGO coating was synthesized from coronene by solution deposition and subsequent annealing. Although SS316L is not a known platform for catalytic growth of graphene-like material, we demonstrated that electrochemical etching increases the free metal concentration on the surface and allows rGO growth. Cytotoxicity studies demonstrate that rGO/SS316L does not have toxic effects on mammalian cells. rGO coatings could significantly improve the mechanical and biological properties, improving the properties of stainless steel for biomedical and biotechnology applications.

Acknowledgements

F.R. and D.M. acknowledge partial salary support from the Canada Research Chairs program. L.C. acknowledges partial salary support through a personal fellowship from FRSQ. F.R. and D.M. are supported through individual Discovery Grants from NSERC. F.R. is grateful to NSERC for an EWR Steacie Memorial Fellowship. We acknowledge funding from FRQNT through a team grant. This research has been enabled by the use of computing resources provided by WestGrid and Compute/Calcul Canada. We thank Mr C. Chabanier for help with contact angle measurements.

Notes and references

1 D. F. Williams, *Biomaterials*, 2008, **29**, 2941–2953.
2 F. Variola, F. Vetrone, L. Richert, P. Jedrzejowski, J.-H. Yi, S. Zalzal, S. Clair, A. Sarkissian, D. F. Perepichka, J. D. Wuest, F. Rosei and A. Nanci, *Small*, 2009, **5**, 996–1006.
3 F. Airoldi, A. Colombo, D. Tavano, G. Stankovic, S. Klugmann, V. Paolillo, E. Bonizzoni, C. Briguori, M. Carlino, M. Montorfano, F. Liistro, A. Castelli, A. Ferrari, F. Sgura and C. Di Mario, *Am. J. Cardiol.*, 2004, **93**, 474–477.
4 C. Bayram, A. K. Mizrak, S. Aktürk, H. Kurşaklioğlu, A. Iyisoy, A. Ifran and E. B. Denkbaş, *Biomed. Mater.*, 2010, **5**, 055007.
5 W. C. Broaddus, K. L. Holloway, C. J. Winters, M. R. Bullock, R. S. Graham, B. E. Mathern, J. D. Ward and H. F. Young, *J. Neurosurg.*, 2002, **96**, 244–247.
6 L. Reclaru, R. Lerf, P. Y. Eschler and J. M. Meyer, *Biomaterials*, 2001, **22**, 269–279.
7 C. N. Kraft, B. Burian, L. Perlick, M. A. Wimmer, T. Wallny, O. Schmitt and O. Diedrich, *J. Biomed. Mater. Res.*, 2001, **57**, 404–412.
8 P. Neumann, C. Bourauel and A. Jäger, *J. Mater. Sci.: Mater. Med.*, 2002, **13**, 141–147.
9 Y. Yonekura, K. Endo, M. Iijima, H. Ohno and I. Mizoguchi, *Dent. Mater. J.*, 2004, **23**, 197–202.
10 O. F. Bertrand, R. Sipehia, R. Mongrain, J. Rodés, J. C. Tardif, L. Bilodeau, G. Côté and M. G. Bourassa, *J. Am. Coll. Cardiol.*, 1998, **32**, 562–571.
11 M. P. Ryan, D. E. Williams, R. J. Chater, B. M. Hutton and D. S. McPhail, *Nature*, 2002, **415**, 770–774.
12 K. Hashimoto, M. Seo, G. Herting, I. Odnevall Wallinder and C. Leygraf, *Corros. Sci.*, 2007, **49**, 103–111.
13 C. Lee, X. Wei, J. W. Kysar and J. Hone, *Science*, 2008, **321**, 385–388.
14 S. Chen, L. Brown, M. Levendorf, W. Cai, S.-Y. Ju, J. Edgeworth, X. Li, C. W. Magnuson, A. Velamakanni, R. D. Piner, J. Kang, J. Park and R. S. Ruoff, *ACS Nano*, 2011, **5**, 1321–1327.
15 D. Prasai, J. C. Tuberquia, R. R. Harl, G. K. Jennings, B. R. Rogers and K. I. Bolotin, *ACS Nano*, 2012, **6**, 1102–1108.
16 F. Zhou, Z. Li, G. J. Shenoy, L. Li and H. Liu, *ACS Nano*, 2013, **7**, 6939–6947.
17 M. Schriver, W. Regan, W. J. Gannett, A. M. Zaniewski, M. F. Crommie and A. Zettl, *ACS Nano*, 2013, **7**, 5763–5768.
18 J. S. Bunch, S. S. Verbridge, J. S. Alden, A. M. van der Zande, J. M. Parpia, H. G. Craighead and P. L. McEuen, *Nano Lett.*, 2008, **8**, 2458–2462.
19 Y. Zhang, T. R. Nayak, H. Hong and W. Cai, *Nanoscale*, 2012, **4**, 3833–3842.
20 K. P. Loh, Q. Bao, G. Eda and M. Chhowalla, *Nat. Chem.*, 2010, **2**, 1015–1024.
21 L. A. L. Tang, J. Wang and K. P. Loh, *J. Am. Chem. Soc.*, 2010, **132**, 10976–10977.
22 A. Sahu, W. Il Choi and G. Tae, *Chem. Commun.*, 2012, **48**, 5820–5822.
23 Y. Wang, W. C. Lee, K. K. Manga, P. K. Ang, J. Lu, Y. P. Liu, C. T. Lim and K. P. Loh, *Adv. Mater.*, 2012, **24**, 4285–4290.
24 Z. Liu, J. T. Robinson, X. Sun and H. Dai, *J. Am. Chem. Soc.*, 2008, **130**, 10876–10877.
25 X. Yang, N. Zhao and F.-J. Xu, *Nanoscale*, 2014, **6**, 6141–6150.
26 A. Bianco, *Angew. Chem., Int. Ed.*, 2013, **52**, 4986–4997.
27 L. Cardenas, J. MacLeod, J. Lipton-Duffin, and F. Rosei, submitted to the *U.S. Patent office*. 61/896,278, 2013, United States.
28 I. Vlassiouk, M. Regmi, P. Fulvio, S. Dai, P. Datskos, G. Eres and S. Smirnov, *ACS Nano*, 2011, **5**, 6069–6076.
29 I. Horcas, R. Fernández, J. M. Gómez-Rodríguez, J. Colchero, J. Gómez-Herrero and A. M. Baro, *Rev. Sci. Instrum.*, 2007, **78**, 013705.
30 C. A. Schneider, W. S. Rasband and K. W. Eliceiri, *Nat. Methods*, 2012, **9**, 671–675.
31 A. F. Stalder, G. Kulik, D. Sage, L. Barbieri and P. Hoffmann, *Colloids Surf., A*, 2006, **286**, 92–103.
32 M. J. Frisch, G. W. Trucks, H. B. Schlegel, G. E. Scuseria, M. A. Robb, J. R. Cheeseman, G. Scalmani, V. Barone, B. Mennucci, G. A. Petersson, H. Nakatsuji, M. Caricato, X. Li, H. P. Hratchian, A. F. Izmaylov, J. Bloino, G. Zheng, J. L. Sonnenberg, M. Hada, M. Ehara, K. Toyota, R. Fukuda, J. Hasegawa, M. Ishida, T. Nakajima, Y. Honda, O. Kitao, H. Nakai, T. Vreven, J. A. Montgomery, J. E. Peralta, F. Ogliaro, M. Bearpark, J. J. Heyd, E. Brothers, K. N. Kudin, V. N. Staroverov, R. Kobayashi,

J. Normand, K. Raghavachari, A. Rendell, J. C. Burant, S. S. Iyengar, J. Tomasi, M. Cossi, N. Rega, J. M. Millam, M. Klene, J. E. Knox, J. B. Cross, V. Bakken, C. Adamo, J. Jaramillo, R. Gomperts, R. E. Stratmann, O. Yazyev, A. J. Austin, R. Cammi, C. Pomelli, J. W. Ochterski, R. L. Martin, K. Morokuma, V. G. Zakrzewski, G. A. Voth, P. Salvador, J. J. Dannenberg, S. Dapprich, A. D. Daniels, Ö. Farkas, J. B. Foresman, J. V. Ortiz, J. Cioslowski and D. J. Fox, *Gaussian 09, Revision B.01*, Gaussian Inc., Wallingford CT, 2009.

33 A. D. Becke, *J. Chem. Phys.*, 1993, **98**, 5648.

34 S. Anoopkumar-Dukie, J. B. Carey, T. Conere, E. O'sullivan, F. N. van Pelt and A. Allshire, *Br. J. Radiol.*, 2005, **78**, 945–947.

35 J. O'Brien, I. Wilson, T. Orton and F. Pognan, *Eur. J. Biochem.*, 2000, **267**, 5421–5426.

36 A. V. Talyzin, S. M. Luzan, K. Leifer, S. Akhtar, J. Fetzer, F. Cataldo, Y. O. Tsybin, C. W. Tai, A. Dzwilewski and E. Moons, *J. Phys. Chem. C*, 2011, **115**, 13207–13214.

37 M. S. Dresselhaus, A. Jorio, M. Hofmann, G. Dresselhaus and R. Saito, *Nano Lett.*, 2010, **10**, 751–758.

38 H. Kuzmany, M. Matus, B. Burger and J. Winter, *Adv. Mater.*, 1994, **6**, 731–745.

39 K. N. Kudin, B. Ozbas, H. C. Schniepp, R. K. Prud'homme, I. A. Aksay and R. Car, *Nano Lett.*, 2008, **8**, 36–41.

40 R. Rao, D. Tishler, J. Katoch and M. Ishigami, *Phys. Rev. B: Condens. Matter Mater. Phys.*, 2011, **84**, 113406.

41 A. Ferrari and J. Robertson, *Phys. Rev. B: Condens. Matter Mater. Phys.*, 2000, **61**, 14095–14107.

42 F. Tuinstra, *J. Chem. Phys.*, 1970, **53**, 1126.

43 I. K. Moon, J. Lee, R. S. Ruoff and H. Lee, *Nat. Commun.*, 2010, **1**, 73.

44 S. Eigler, C. Dotzer and A. Hirsch, *Carbon*, 2012, **50**, 3666–3673.

45 I. Jung, J.-S. Rhyee, J. Y. Son, R. S. Ruoff and K.-Y. Rhee, *Nanotechnology*, 2012, **23**, 025708.

46 D. L. Duong, G. H. Han, S. M. Lee, F. Gunes, E. S. Kim, S. T. Kim, H. Kim, Q. H. Ta, K. P. So, S. J. Yoon, S. J. Chae, Y. W. Jo, M. H. Park, S. H. Chae, S. C. Lim, J. Y. Choi and Y. H. Lee, *Nature*, 2012, **490**, 235–239.

47 M. Haïdopoulos, S. Turgeon, G. Laroche and D. Mantovani, *Plasma Processes Polym.*, 2005, **2**, 424–440.

48 A. Lerf, H. He, M. Forster and J. Klinowski, *J. Phys. Chem. B*, 1998, **102**, 4477–4482.

49 D. W. Boukhvalov and M. I. Katsnelson, *J. Am. Chem. Soc.*, 2008, **130**, 10697–10701.

50 R. John, A. Ashokreddy, C. Vijayan and T. Pradeep, *Nanotechnology*, 2011, **22**, 165701.

51 J.-T. Chi, H. Y. Chang, G. Haraldsen, F. L. Jahnsen, O. G. Troyanskaya, D. S. Chang, Z. Wang, S. G. Rockson, M. van de Rijn, D. Botstein and P. O. Brown, *Proc. Natl. Acad. Sci. U. S. A.*, 2003, **100**, 10623–10628.

52 A. Schreer, C. Tinson, J. P. Sherry and K. Schirmer, *Anal. Biochem.*, 2005, **344**, 76–85.

